Calculation of the SAR Induced in Head Tissues Using a High Order DGTD Method and Triangulated Geometrical Models

Hassan Fahs [#1], Stéphane Lanteri [#2], Joe Wiart [*3], Man-Fai Wong [*4]

[#] NACHOS *project-team, INRIA Sophia Antipolis-Méditerranée research center*
2004 Route des Lucioles, BP 93, 06902 Sophia Antipolis Cedex, France
[1] Hassan.Fahs@inria.fr
[2] Stephane.Lanteri@inria.fr

[*] *Orange Labs R&D, WHIST Laboratory*
38/40 Rue du Général Leclerc, 92794 Issy-les-Moulineaux Cedex 9, France
[3] joe.wiart@orange-ftgroup.com
[4] manfai.wong@orange-ftgroup.com

***Abstract*—The great majority of numerical calculations of the Specific Absorption Rate (SAR) induced in human tissues exposed to microwaves are performed using the Finite Difference Time Domain (FDTD) method and voxel based geometrical models. The straightforward implementation of the method and its computational efficiency are among the main reasons for FDTD being currently the leading method for numerical assessment of human exposure to electromagnetic waves. However, the rather difficult departure from the commonly used cartesian grid and cell size limitations regarding the discretization of very detailed structures of human tissues are often recognized as the main weaknesses of the method in this application context. We present here an alternative numerical dosimetry methodology combining a high order Discontinuous Galerkin Time Domain (DGTD) method and adapted geometrical models based on unstructured triangulations, and discuss its application to the calculation of the SAR induced in head tissues.**

I. INTRODUCTION

Nowadays, numerical modeling is increasingly used and progressively becoming a mandatory path for the study of the interaction of electromagnetic fields with biological tissues. This is for instance the case for the evaluation of the distribution of the SAR which is a measure of the rate at which electric energy is absorbed by the tissues when exposed to a radio-frequency electromagnetic field. The SAR is defined as the power absorbed per mass of tissue and has units of watts per kilogram. It is usually averaged either over the whole body, or over a small sample volume (typically 1g or 10g of tissue). Such SAR calculations are at the basis of numerical dosimetry studies of the exposure of human tissues to microwave radiations from wireless communication systems [1]- [2]- [3]. These studies are useful for assessing the possible thermal effects (temperature rise in tissues resulting from electric energy dissipation) as well as for compliance testing to regulatory limits.

Despite the high complexity both in terms of heterogeneity and geometrical features of tissues, the great majority of numerical dosimetry studies have been conducted using the widely known FDTD method due to Yee [4]. In this method, the whole computational domain is discretized using a structured (cartesian) grid. Due to the possible straightforward implementation of the algorithm and the availability of computational power, FDTD is currently the leading method for numerical assessment of human exposure to electromagnetic waves. In the particular case of mobile phone radiation, numerical dosimetry studies are conducted by solving the system of Maxwell equations on heterogeneous discretized models of human head tissues built from medical images. Thus, the grid generation process is highly simplified since the voxel based image can be used at a minimal effort as the computational grid for the FDTD method. In spite of its flexibility and second-order accuracy in a homogeneous medium, the Yee scheme suffers from serious accuracy degradation when used to model curved objects or when treating material interfaces.

In an attempt to offer an alternative numerical dosimetry methodology which allows for a realistic modeling of geometrical features and tissue interfaces, we consider here the use of a discontinuous finite element method formulated on non-uniform tetrahedral meshes. The method is known as the discontinuous Galerkin method and has been studied by several authors rather recently for solving the time-domain Maxwell equations [5]- [6]- [7]. Discontinuous Galerkin time-domain (DGTD) methods based on discontinuous finite element spaces, easily handle elements of various types and shapes, irregular non-conforming meshes [8], and even locally varying polynomial degree, and hence offer great flexibility in the mesh design. They also lead to (block-) diagonal mass matrices and therefore yield fully explicit, inherently parallel methods when coupled with explicit time stepping.

II. HIGH ORDER DGTD METHOD

A. Continuous Problem

We consider the Maxwell equations in three space dimensions for heterogeneous linear isotropic media. The elec-

tric field $\vec{E}(\vec{x},t) = {}^t(E_x,E_y,E_z)$ and the magnetic field $\vec{H}(\vec{x},t) = {}^t(H_x,H_y,H_z)$ verify:

$$\epsilon\partial_t\vec{E} - \text{curl}\vec{H} = -\vec{J}, \quad \mu\partial_t\vec{H} + \text{curl}\vec{E} = 0, \tag{1}$$

where the symbol ∂_t denotes a time derivative and $\vec{J}(\vec{x},t)$ is a current source term. These equations are set on a bounded polyhedral domain Ω of $\mathbb{R}^3$. The permittivity $\epsilon(\vec{x})$ and the magnetic permeability tensor $\mu(\vec{x})$ are varying in space, time-invariant and both positive functions. Our goal is to solve system (1) in a domain Ω with boundary $\partial\Omega = \Gamma_a \cup \Gamma_m$, where we impose the following boundary conditions:

$$\vec{n}\times\vec{E} = 0 \text{ on } \Gamma_m, \quad \mathcal{L}(\vec{E},\vec{H}) = \mathcal{L}(\vec{E}_{\text{inc}},\vec{H}_{\text{inc}}) \text{ on } \Gamma_a, \tag{2}$$

where $\mathcal{L}(\vec{E},\vec{H}) = \vec{n}\times\vec{E} - \sqrt{\frac{\mu}{\varepsilon}}\vec{n}\times(\vec{H}\times\vec{n})$. Here $\vec{n}$ denotes the unit outward normal to $\partial\Omega$ and $(\vec{E}_{\text{inc}},\vec{H}_{\text{inc}})$ is a given incident field. The first boundary condition is called *metallic* (referring to a perfectly conducting surface) while the second condition is called *absorbing* and takes here the form of the Silver-Müller condition which is a first order approximation of the exact absorbing boundary condition. This absorbing condition is applied on Γ_a which represents an artificial truncation of the computational domain.

B. Discretization in Space

We consider a partition $\mathcal{T}_h$ of Ω into a set of tetrahedra τ_i with boundary $\partial\tau_i$. For each τ_i, ϵ_i and μ_i are respectively the local electric permittivity and magnetic permeability of the medium, which are assumed constant inside the element τ_i. For two distinct tetrahedra τ_i and τ_k in $\mathcal{T}_h$, the intersection $\tau_i \cap \tau_k$ is a triangle a_{ik} which we will call interface. For each internal interface a_{ik}, we denote by $\vec{n}_{ik}$ the unitary normal vector, oriented from τ_i to τ_k. Finally, we denote by $\mathcal{V}_i$ the set of indices of the elements which are neighbors of τ_i (having an interface in common). In the following, to simplify the presentation, we set $\vec{J} = 0$. For a given partition $\mathcal{T}_h$, we seek approximate solutions to (1) in the finite dimensional subspace $V_{p_i}(\mathcal{T}_h) = \{\vec{v} \in L^2(\Omega)^3 : \vec{v}_{|\tau_i} \in (\mathbb{P}_{p_i}(\tau_i))^3 \quad \forall\tau_i \in \mathcal{T}_h\}$ where $\mathbb{P}_{p_i}(\tau_i)$ denotes the space of nodal polynomial functions of degree at most p_i inside the element τ_i. Following the discontinuous Galerkin approach, the electric and magnetic fields inside each finite element are seeked for as linear combinations $(\vec{\mathbf{E}}_i,\vec{\mathbf{H}}_i)$ of linearly independent basis vector fields $\vec{\varphi_{ij}}$, $1 \le j \le d_i$, where d_i denotes the local number of degrees of freedom inside τ_i. Let $\mathcal{P}_i = \text{Span}(\vec{\varphi_{ij}},\ 1 \le j \le d_i)$. The approximate fields $(\vec{\mathbf{E}}_h,\vec{\mathbf{H}}_h)$, defined by $(\forall i, \vec{\mathbf{E}}_{h|\tau_i} = \vec{\mathbf{E}}_i, \vec{\mathbf{H}}_{h|\tau_i} = \vec{\mathbf{H}}_i)$ are allowed to be completely discontinuous across element boundaries. For such a discontinuous field $\vec{\mathbf{U}}_h$, we define its average $\{\vec{\mathbf{U}}_h\}_{ik}$ through any internal interface a_{ik}, as $\{\vec{\mathbf{U}}_h\}_{ik} = (\vec{\mathbf{U}}_{i|a_{ik}} + \vec{\mathbf{U}}_{k|a_{ik}})/2$. Because of this discontinuity, a global variational formulation cannot be obtained. Instead, we dot-multiply (1) by a vector function $\vec{\varphi} \in \mathcal{P}_i$, integrate over each single element τ_i and integrate by parts. Then, for integrals over $\partial\tau_i$, a specific treatment must be introduced since the approximate fields are discontinuous through element faces, leading to the definition of a *numerical flux*. We choose to use a fully centered numerical flux, *i.e.* $\forall i,\forall k \in \mathcal{V}_i$, $\vec{\mathbf{E}}_{|a_{ik}} \simeq \{\vec{\mathbf{E}}_h\}_{ik}$, $\vec{\mathbf{H}}_{|a_{ik}} \simeq \{\vec{\mathbf{H}}_h\}_{ik}$. The metallic boundary condition (first relation of (2)) on a boundary interface $a_{ik} \in \Gamma_m$ (k in the element index of the fictitious neighboring element) is dealt with *weakly*, in the sense that traces of fictitious fields $\vec{\mathbf{E}}_k$ and $\vec{\mathbf{H}}_k$ are used for the computation of numerical fluxes for the boundary element τ_i. More precisely, we set $\vec{\mathbf{E}}_{k|a_{ik}} = -\vec{\mathbf{E}}_{i|a_{ik}}$ and $\vec{\mathbf{H}}_{k|a_{ik}} = \vec{\mathbf{H}}_{i|a_{ik}}$. Similary, the absorbing boundary condition (second relation of (2)) is taken into account through the use of a fully upwind numerical flux for the evaluation of the corresponding boundary integral over $a_{ik} \in \Gamma_a$ (see [9] for more details). This yields:

$$\left\{\begin{array}{l} \displaystyle\int_{\tau_i} \vec{\varphi}\cdot\epsilon_i\partial_t\vec{\mathbf{E}}_i = \frac{1}{2}\int_{\tau_i}(\text{curl}\vec{\varphi}\cdot\vec{\mathbf{H}}_i + \text{curl}\vec{\mathbf{H}}_i\cdot\vec{\varphi}) \\ \qquad\qquad\qquad - \displaystyle\frac{1}{2}\sum_{k\in\mathcal{V}_i}\int_{a_{ik}}\vec{\varphi}\cdot(\vec{\mathbf{H}}_k\times\vec{n}_{ik}), \\ \displaystyle\int_{\tau_i} \vec{\varphi}\cdot\mu_i\partial_t\vec{\mathbf{H}}_i = -\frac{1}{2}\int_{\tau_i}(\text{curl}\vec{\varphi}\cdot\vec{\mathbf{E}}_i + \text{curl}\vec{\mathbf{E}}_i\cdot\vec{\varphi}) \\ \qquad\qquad\qquad + \displaystyle\frac{1}{2}\sum_{k\in\mathcal{V}_i}\int_{a_{ik}}\vec{\varphi}\cdot(\vec{\mathbf{E}}_k\times\vec{n}_{ik}). \end{array}\right. \tag{3}$$

Eq. (3) can be rewritten in terms of scalar unknowns. Inside each element, the fields are recomposed according to $\vec{\mathbf{E}}_i = \sum_{1\le j\le d} E_{ij}\vec{\varphi}_{ij}$ and $\vec{\mathbf{H}}_i = \sum_{1\le j\le d} H_{ij}\vec{\varphi}_{ij}$ and let us now denote by $\mathbf{E}_i$ and $\mathbf{H}_i$ respectively the column vectors $(E_{il})_{1\le l\le d}$ and $(H_{il})_{1\le l\le d}$. Then, (3) is equivalent to:

$$\left\{\begin{array}{rcl} M_i^\epsilon\dfrac{d\mathbf{E}_i}{dt} &=& K_i\mathbf{H}_i - \displaystyle\sum_{k\in\mathcal{V}_i} S_{ik}\mathbf{H}_k, \\ M_i^\mu\dfrac{d\mathbf{H}_i}{dt} &=& -K_i\mathbf{E}_i + \displaystyle\sum_{k\in\mathcal{V}_i} S_{ik}\mathbf{E}_k, \end{array}\right. \tag{4}$$

where the symmetric positive definite mass matrices M_i^σ (σ stands for ϵ or μ) are local (element-wise) mass matrices, K_i is the local stiffness matrix and S_{ik} are interface matrices.

C. Time Discretization

The semidiscrete system (4) is time integrated using a second-order leap-frog scheme as:

$$\left\{\begin{array}{rcl} M_i^\epsilon\left(\dfrac{\mathbf{E}_i^{n+1}-\mathbf{E}_i^n}{\Delta t}\right) &=& K_i\mathbf{H}_i^{n+\frac{1}{2}} - \displaystyle\sum_{k\in\mathcal{V}_i} S_{ik}\mathbf{H}_k^{n+\frac{1}{2}}, \\ M_i^\mu\left(\dfrac{\mathbf{H}_i^{n+\frac{3}{2}}-\mathbf{H}_i^{n+\frac{1}{2}}}{\Delta t}\right) &=& -K_i\mathbf{E}_i^{n+1} + \displaystyle\sum_{k\in\mathcal{V}_i} S_{ik}\mathbf{E}_k^{n+1}. \end{array}\right.$$

The resulting fully explicit DGTD-$\mathbb{P}_{p_i}$ method is analyzed in [6] where it is shown that the method is non-dissipative, conserves a discrete form of the electromagnetic energy and is stable under a CFL-like.

III. Tetrahedral Mesh Based Geometric Models of Head Tissues

The DGTD-$\mathbb{P}_{p_i}$ method described previously assumes that the computational domain is discretized using tetrahedral elements. In this study, we aim at exploiting this numerical method for the calculation of the SAR induced in head tissues. A first step is thus to construct compatible geometrical models of the head tissues. The Visible Human project [1] aimed at the construction of complete, anatomically detailed, three-dimensional representations of male and female human bodies. Among other achievements, high resolution images of representative male and female cadavers have been completed. These image data sets are used for various research purposes among which numerical dosimetry studies of human tissues exposure to electromagnetic fields. As a matter of fact, the Visible Human model is now used by several groups world-wide involved in such studies.

Starting from magnetic resonance images of the Visible Human 2.0 project [10], head tissues are segmented and the interfaces of a selected number of tissues are triangulated. Different strategies can be used in order to obtain a smooth and accurate segmentation of head tissues and interface triangulations as well. A first strategy consists in using a marching cube algorithm [11] which leads to huge triangulations of interfaces between segmented subdomains. These triangulations can then be regularized, refined and decimated in order to obtain reasonable surface meshes, for example using the YAMS [12] re-meshing tool. Another strategy consists in using a variant of Chew's algorithm [13], based on Delaunay triangulation restricted to the interface, which allows to control the size and aspect ratio of interfacial triangles [14]. Example of triangulations of the skin and the skull, are shown on Fig. 1. Then, these triangulated surfaces together with a triangulation of the artificial boundary (absorbing boundary) of the overall computational domain are used as inputs for the generation of volume meshes. Finally, the GHS3D tetrahedral mesh generator [15] is used to mesh the volume domains between the various interfaces. The exterior of the head must also be meshed, up to a certain distance, where an artificial absorbing boundary condition has to be set. Moreover, a simplified mobile phone model (metallic box with a quarter-wave length mounted on the top surface) is included and placed in vertical position close to the right ear. Overall, the geometrical models considered here consist of four tissues (skin, skull, CSF - Cerebro Spinal Fluid and brain).

IV. Numerical Results

All the numerical experiments reported here are concerned with the propagation of an electromagnetic wave emitted by a dipolar source localized (and centered) between the lower tip of the antenna and the top surface of the mettalic box, and is modeled by a current of the form ($\vec{x}_d$ is the localization point of the source) $J_z^d(\vec{x},t) = \delta(\vec{x}-\vec{x}_d)f(t)$ where $f(t)$ is sinusoidally varying temporal signal with frequency F=1800 MHz. This source current is easily introduced and discretized according to the discontinuous Galerkin formulation discussed in subsection II-B. A discrete Fourier transform of the components of the electric field is computed during the last period of the simulation.

[1] http://www.nlm.nih.gov/research/visible/visible_human.html

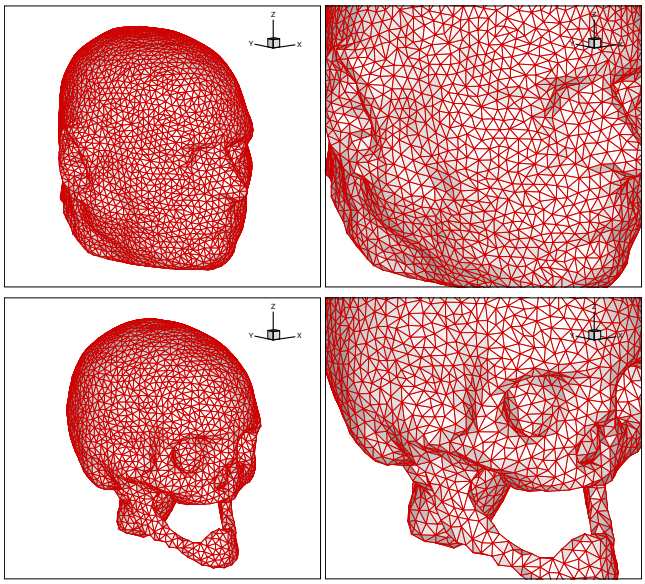

Fig. 1: Surface meshes of the skin (top) and the skull (bottom).

We consider a sequence of three meshes whose characteristics are summarized in Table I. For these meshes, the artificial boundary Γ_a is a spherical surface approximately located one wavelength away from the skin. The tetrahedral meshes are globally non-uniform and the quantities L_{min}, L_{max} and L_{avg} in Table I respectively denote the minimum, maximum and average length of mesh edges. Numerical simulations have been performed for a duration of 5 periods of the source signal. Contour lines of the local SAR normalized to the maximum value of the local SAR one one hand, and of the local SAR normalized to the total emitted power on the other hand, are shown in Fig. 2 for the calculations based on mesh M3. Finally, Table II summarizes the values of the local SAR normalized to the total emitted power.

TABLE I: Characteristics of the tetrahedral meshes of head tissues for calculations with the DGTD-$\mathbb{P}_p$ method.

Mesh	# elements	L_{min} (mm)	L_{max} (mm)	L_{avg} (mm)
M1	815,405	1.00	28.14	10.69
M2	1,862,136	0.65	23.81	6.89
M3	7,894,172	0.77	22.75	3.21

In the following, we consider that the approximate solution computed with mesh M3 using the DGTD-$\mathbb{P}_1$ method defines a reference solution. Patterns of the contour lines for calculations respectively performed with mesh M1 using the DGTD-$\mathbb{P}_3$ method, with mesh M2 using the DGTD-$\mathbb{P}_2$ method on one hand (not shown here), and with mesh M3 using the DGTD-$\mathbb{P}_1$ method on the other hand, are very similar. In Table II,

the quantity given parenthetically is the difference with the reference value (*i.e.* the one associated to mesh M3 and the DGTD-$\mathbb{P}_1$ method) and the corresponding error level. We note here that the relative error tends to increase when switching from $p = 1$ to $p = 2$ for a given discretization mesh. Again, this should not be interpreted as a counter effect of an increase of the approximation order since this relative error is evaluated on the basis of a solution computed on the finest mesh which is based on high resolution triangulations of the tissue interfaces (see the figures in section III). Rather, we can surely conclude that the discretization of the geometrical features of tissues has a greater impact on accuracy than the interpolation order in the DGTD-$\mathbb{P}_p$ method.

TABLE II: Calculations with the DGTD-$\mathbb{P}_p$ method. Maximum value of the normalized local SAR.

Mesh	DGTD-$\mathbb{P}_1$
M1	3.365 W/Kg (0.463, 12.1 %)
M2	3.734 W/Kg (0.094, 2.4 %)
M3	3.828 W/Kg
Mesh	DGTD-$\mathbb{P}_2$
M1	3.269 W/Kg (0.559, 14.6 %)
M2	3.586 W/Kg (0.242, 6.3 %)
Mesh	DGTD-$\mathbb{P}_3$
M1	3.283 W/Kg (0.545, 12.3 %)

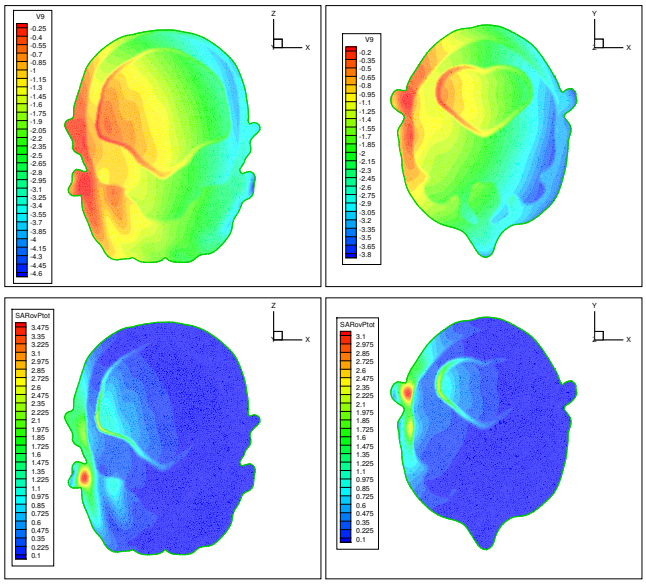

Fig. 2: Calculations with the DGTD-$\mathbb{P}_1$ method. Mesh M3: contour lines of local SAR over maximum local SAR in log scale (top) and the normalized local SAR (bottom) in selected cut planes).

We conclude this results section by summarizing in Table III the computing times of the calculations reported here. Numerical simulations have been conducted on a Bull Novascale 3045 parallel system consisting of Intel Itanium 2/1.6 GHz nodes interconnected by a high performance Infiniband network. Each node consists of a 8 core board with 21 GB of shared memory. The parallelization of the DGTD-$\mathbb{P}_p$ method relies on a SPMD (Single Program Multiple Data) strategy which combines a partitioning of the tetrahedral mesh with a message passing programming using the MPI interface.

TABLE III: Calculations with the DGTD-$\mathbb{P}_p$ method. Computing times (the quantity given parenthetically is the number of processing units).

Mesh	DGTD-$\mathbb{P}_1$	DGTD-$\mathbb{P}_2$	DGTD-$\mathbb{P}_3$
M1	570 s (128)	707 s (128)	1862 s (128)
M2	239 s (256)	1142 s (256)	-
M3	761 s (512)	-	

ACKNOWLEDGMENT

This work was granted access to the HPC resources of CCRT under the allocation 2009-t2009065004 made by GENCI (Grand Equipement National de Calcul Intensif).

REFERENCES

[1] P. Bernardi, M. Cavagnaro, S. Pisa, and E. Piuzzi, "Specific absorption rate and temperature increases in the head of a cellular phone user," *IEEE Trans. Microwave Theory Tech.*, vol. 48, no. 7, pp. 1118–1126, 2000.

[2] ——, "Power absorption and temperature elevations induced in the human head by a dual-band monopole-helix antenna phone," *IEEE Trans. Microwave Theory Tech.*, vol. 49, no. 12, pp. 2539–2546, 2001.

[3] O. Gandhi, Q.-X. Li, and G. Kang, "Temperature rise for the human head for cellular telephones and for peak SARs prescribed in safety guidelines," *IEEE Trans. Microwave Theory Tech.*, vol. 49, no. 9, pp. 1607–1613, 2001.

[4] K. Yee, "Numerical solution of initial boundary value problems involving Maxwell's equations in isotropic media," *IEEE Trans. Antennas and Propagation*, vol. AP-16, pp. 302–307, 1966.

[5] J. Hesthaven and T. Warburton, "Nodal high-order methods on unstructured grids. I. Time-domain solution of Maxwell's equations," *J. Comput. Phys.*, vol. 181, pp. 186–221, 2002.

[6] L. Fezoui, S. Lanteri, S. Lohrengel, and S. Piperno, "Convergence and stability of a discontinuous Galerkin time-domain method for the 3D heterogeneous Maxwell equations on unstructuredmeshes," *ESAIM: Math. Model. Numer. Anal.*, vol. 39, no. 6, pp. 1149–1176, 2005.

[7] G. Cohen, X. Ferrieres, and S. Pernet, "A spatial high-order hexahedral discontinuous Galerkin method to solve Maxwell's equations in time domain," *J. Comput. Phys.*, vol. 217, pp. 340–363, 2006.

[8] H. Fahs, "Development of a hp-like discontinuous Galerkin time-domain method on non-conforming simplicial meshes for electromagnetic wave propagation," *Int. J. Numer. Anal. Mod.*, vol. 6, no. 2, pp. 193–216, 2009.

[9] A. Catella, V. Dolean, and S. Lanteri, "An implicit discontinuous Galerkin time-domain method for two-dimensional electromagnetic wave propagation," *COMPEL*, 2009, to appear.

[10] P. Ratiu, B. Hillen, J. Glaser, and D. Jenkins, *Medicine Meets Virtual Reality 11 - NextMed: Health Horizon*. IOS Press, 2003, vol. 11, ch. Visible Human 2.0 - the next generation, pp. 275–281.

[11] W. Lorensen and H. Cline, "Marching cubes: a high resolution 3D surface construction algorithm," in *Siggraph 87*, vol. 21, 1987, pp. 163–170.

[12] P. Frey, "YAMS: a fully automatic adaptive isotropic surface remeshing procedure," INRIA Technical Report RT-0252, Tech. Rep., 2001.

[13] L. Chew, "Guaranteed-quality mesh generation for curved surfaces," in *9th Annual ACM Symposium Computational Geometry*. ACM Press, 1993, pp. 274–280.

[14] J.-D. Boissonnat and S. Oudot, "Provably good sampling and meshing of surfaces," *Graphical Models*, vol. 67, no. 5, pp. 405–451, 2005.

[15] P.-L. George, F. Hecht, and E. Saltel, "Automatic mesh generator with specified boundary," *Comput. Methods Appl. Mech. Engrg.*, vol. 92, pp. 269–288, 1991.